$\mathcal{PT}$ spectroscopy of the Rabi problem

Yogesh N. Joglekar[1], Rahul Marathe[2], P. Durganandini[2], and Rajeev K. Pathak[2]
[1]*Department of Physics, Indiana University Purdue University Indianapolis (IUPUI), Indianapolis, Indiana 46202, USA*
[2]*Department of Physics, University of Pune, Ganeshkhind, Pune 411007, India*
(Dated: July 18, 2014)

We investigate the effects of a time-periodic, non-hermitian, $\mathcal{PT}$-symmetric perturbation on a system with two (or few) levels, and obtain its phase diagram as a function of the perturbation strength and frequency. We demonstrate that when the perturbation frequency is close to one of the system resonances, even a vanishingly small perturbation leads to $\mathcal{PT}$ symmetry breaking. We also find a restored $\mathcal{PT}$-symmetric phase at high frequencies, and at moderate perturbation strengths, we find multiple frequency windows where $\mathcal{PT}$-symmetry is broken and restored. Our results imply that the $\mathcal{PT}$-symmetric Rabi problem shows surprisingly rich phenomena absent in its hermitian or static counterparts.

arXiv:1407.4535v1 [physics.optics] 17 Jul 2014

Introduction. A two-level system coupled to a sinusoidally varying potential is a prototypical example of a time-dependent, exactly solvable Hamiltonian, with profound implications to atomic, molecular, and optical physics [1]. When the frequency of perturbation ω is close to the characteristic frequency Δ of the two-level system - near resonance - the system undergoes complete population inversion for an arbitrarily small strength γ of the potential [2]. The implications of this result to spin magnetic resonance, Rabi flopping [3], and its generalization, namely the Jaynes-Cummings model [4, 5], have been extensively studied over the past half century [6, 7]. Surprisingly, the quantum Rabi problem, where the full quantum nature of the perturbing bosonic field is taken into account, has only been recently solved [8].

The two-level model is useful because it is applicable to many-level systems when the perturbation frequency is close to or resonant with a *single pair of levels*. As the detuning away from resonance $|\Delta - \omega|$ increases, the perturbation strength necessary for population inversion increases linearly with it; in a many-level system, with increased potential strength, transitions to other levels have to be taken into account and the resultant problem is not exactly solvable. Therefore, understanding the behavior of a system in the entire parameter space (γ, ω) requires analytical and numerical approaches. All of these studies are restricted to hermitian potentials.

In recent years, discrete Hamiltonians with a hermitian tunneling term H_0 and a non-hermitian perturbation V that are invariant under combined parity and time-reversal ($\mathcal{PT}$) operations have been extensively investigated [9–16]. The spectrum ϵ_λ of a $\mathcal{PT}$-symmetric Hamiltonian is real when the strength γ of the non-hermitian perturbation is smaller than a threshold γ_{PT} set by the hermitian tunneling term. Traditionally, the emergence of complex-conjugate eigenvalues that occurs when the threshold is exceeded, $\gamma > \gamma_{PT}$, is called $\mathcal{PT}$ symmetry breaking [17–19]. It is now clear that $\mathcal{PT}$-symmetric Hamiltonians represent open systems with balanced gain and loss, and $\mathcal{PT}$ symmetry breaking is a transition from a quasiequilibrium state ($\mathcal{PT}$-symmetric state) to a state with broken reciprocity ($\mathcal{PT}$-broken state) [20]. Recent experiments on optical waveguides [21–23] and resonators [24] with amplification and absorption have shown that $\mathcal{PT}$ systems display a wealth of novel phenomena [25, 26] that are absent in closed or purely dissipative systems. We note that all experiments and most of the theoretical work, with few exceptions [27–29], have only explored systems with static gain and loss potentials.

And what of a system perturbed by a time-periodic gain-loss potential $V(t)$? What is the criterion for $\mathcal{PT}$-symmetry breaking? What is the analog of Rabi flopping in such a case? We answer these questions by investigating small, N-site lattices perturbed by a pair of balanced gain-loss potentials $\pm i\gamma\cos(\omega t)$ located at parity symmetric sites. Such systems can be realized in coupled waveguides with a complex refractive index [22, 23, 28] that varies along the propagation direction, or in coupled resonators [24].

Our primary results are as follows: i) The system can be in "$\mathcal{PT}$-broken phase" even if the spectrum $\epsilon_\lambda(t)$ of the Hamiltonian $H(t)$ is real at all times. ii) Near every resonance, the $\mathcal{PT}$ symmetric threshold is reduced from its static value γ_{PT} to the detuning, $\gamma_{PT}(\omega) \propto |\omega - \Delta|$; in particular, it vanishes at the resonance. iii) For any gain-loss strength including $\gamma \gg \gamma_{PT}$, the $\mathcal{PT}$-symmetric phase is restored at high frequencies $\omega > \omega_c \propto \gamma$. iv) At intermediate strengths, $\gamma \sim \gamma_{PT}$, the $\mathcal{PT}$ symmetry is broken in multiple windows in the frequency domain. Thus, a harmonic, $\mathcal{PT}$-symmetric perturbation provides a new spectroscopic tool for investigating the level structure of a system.

$\mathcal{PT}$ phase diagram. The Hamiltonian for an N-site lattice with constant tunneling is

$$H_0 = -\hbar J \sum_{x=1}^{N-1} \left(|x\rangle\langle x+1| + |x+1\rangle\langle x| \right), \qquad (1)$$

where $|x\rangle$ is a normalized state localized on site x, J is the tunneling rate, and $\hbar = h/(2\pi)$ is the scaled Planck's constant. The action of the parity operator on the lattice

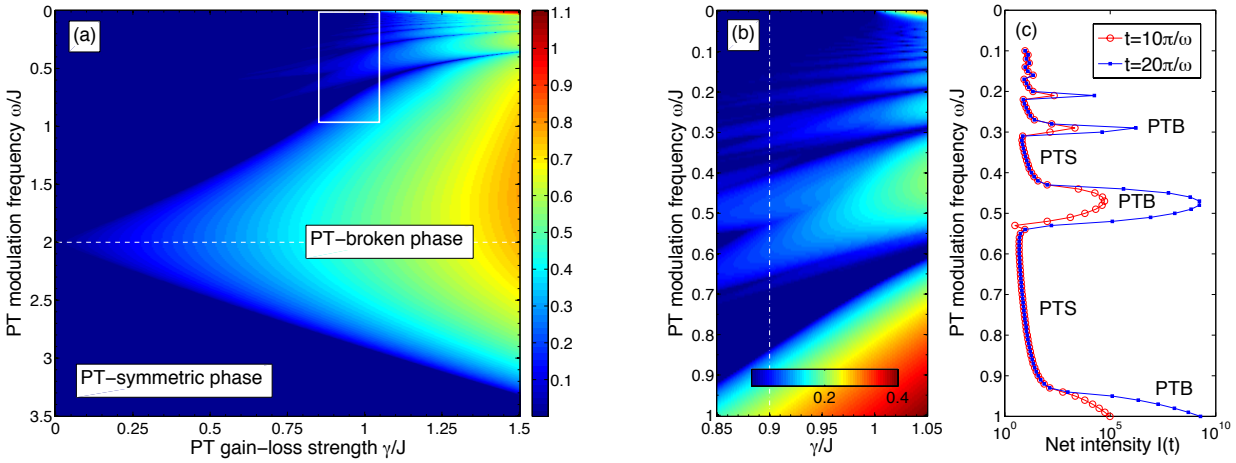

FIG. 1. (color online) (a) $\mathcal{PT}$ phase diagram of a two-level system in the (γ, ω) plane; plotted is the largest imaginary part of the spectrum of $\mathcal{H}$. The static threshold $\gamma_{PT}/J = 1$ is suppressed down to zero when the perturbation frequency matches a resonance, $\omega/J = 2$. (b) A close-up of the area marked by the white rectangle in panel (a) shows that for moderate $\gamma/J \sim 1$, multiple $\mathcal{PT}$-symmetric (PTS) and $\mathcal{PT}$-broken (PTB) regions occur when ω is varied. (c) Maximum of the net intensity $I(t) = \langle\psi(0)|G^\dagger(t)G(t)|\psi(0)\rangle$ at two cutoff times $t = 10\pi/\omega$ (open red circles) and $t = 20\pi/\omega$ (solid blue squares), on horizontal logarithmic axis, as a function of ω on the vertical axis, at $\gamma/J = 0.9$ (white dot-dashed line in panel (b)). PTB regions are distinguished by a clear dependence of $I_{\max}$ on the cutoff.

is given by $x \to \bar{x} = N + 1 - x$ and the antilinear time-reversal operator acts as $i \to -i$. The spectrum of H_0 is given by $\epsilon_n = -2\hbar J\cos(k_n) = -\epsilon_{\bar{n}}$ and the normalized eigenfunctions are $\psi_n(x) = \langle x|n\rangle = \sin(k_n x)/\sqrt{1 + 1/N}$ where $k_n = n\pi/(N + 1)$ with $1 \le n \le N$. The energy differences $\hbar\Delta_{nm} = \epsilon_n - \epsilon_m > 0$ define the possible resonances for this N-level system. Motivated by the Rabi problem, here we will only consider $N = \{2, 3, 4\}$. This system is perturbed by a balanced gain-loss potential

$$V(t) = i\hbar\gamma\cos(\omega t)\left(|x_0\rangle\langle x_0| - |\bar{x}_0\rangle\langle\bar{x}_0|\right) \neq V^\dagger(t). \quad (2)$$

Eq.(2) implies that at time $t = 0$, x_0 is the gain or amplification site and $\bar{x}_0$ is the loss or absorption site. The non-hermitian potential satisfies $\mathcal{PT}V(t)\mathcal{PT} = V(t)$. The total Hamiltonian $H(t) = H_0 + V(t)$ is periodic in time, i.e. $H(t + 2\pi/\omega) = H(t)$, and its properties are best analyzed via its Floquet counterpart, $\mathcal{H} = -i\hbar\partial_t + H$ [30–32]. In the frequency domain, the non-Hermitian, $\mathcal{PT}$-symmetric Floquet Hamiltonian is given by

$$\mathcal{H}^{p,q}_{x,x'} = -ip\hbar\omega\delta_{p,q}\delta_{x,x'} - \delta_{p,q}\hbar J(\delta_{x,x'+1} + \delta_{x,x'-1}) + i\hbar\gamma\delta_{x,x'}(\delta_{p,q+1} + \delta_{p,q-1})(\delta_{x,x_0} - \delta_{x,\bar{x}_0}) \quad (3)$$

where $p, q \in \mathbb{Z}$ denote the Floquet band indices. In practice, a truncated Floquet Hamiltonian with $|p| \le N_f$ is used, so that $\mathcal{H}$ is an $N(2N_f + 1) \times N(2N_f + 1)$ matrix.

We define $\mathcal{PT}$-symmetry breaking as *the emergence of complex-conjugate eigenvalues for the Floquet Hamiltonian* $\mathcal{H}$ [27]. As we will show below, this can occur even if the instantaneous eigenvalues $\epsilon_\lambda(t)$ of the time-dependent Hamiltonian $H(t)$ are purely real over the entire period $T_\omega = 2\pi/\omega$.

Figure 1 is the $\mathcal{PT}$-symmetric phase diagram of a two-level system in the (γ, ω) plane. Figure 1(a) shows the maximum imaginary part of the spectrum of the Hamiltonian $\mathcal{H}$ with 101 Floquet bands. The region with zero imaginary part (dark blue) is the $\mathcal{PT}$-symmetric phase and the region with nonzero imaginary part (all other colors) is the $\mathcal{PT}$-broken phase; the static, $\omega = 0$, threshold is given by $\gamma_{PT}/J = 1$. Figure. 1(a) has three universal features that appear in systems with larger N as well. The first is a vanishingly small $\mathcal{PT}$-symmetric threshold $\gamma_{PT}(\omega)$ that occurs when ω is close to the single resonance frequency for the system, $\Delta_{21} = 2J$. The second is the the emergence of $\mathcal{PT}$-symmetric phase that occurs at large frequencies [29] $\omega > \omega_c \propto \gamma$ for any gain-loss strength including $\gamma/J \ge 1$. The third feature is the presence of multiple windows along the frequency axis such that the $\mathcal{PT}$-symmetry is broken within each window. Fig. 1(b) is a higher resolution close-up of the parameter space marked by the white rectangle in Fig. 1(a). It shows that for a fixed γ, as the frequency of the $\mathcal{PT}$ potential is changed, multiple $\mathcal{PT}$-symmetric and $\mathcal{PT}$-broken regions emerge. *These regions are present both below and above the static threshold.*

A complementary method to distinguish the $\mathcal{PT}$-broken (PTB) region from the $\mathcal{PT}$-symmetric (PTS) region is to track the net intensity $I(t) = \langle\psi(t)|\psi(t)\rangle = \langle\psi(0)|G^\dagger(t)G(t)|\psi(0)\rangle$ of an initially normalized state $|\psi(0)\rangle$. We obtain the non-unitary time-evolution operator

$$G(t) = Te^{-\frac{i}{\hbar}\int_0^t dt' H(t')} \approx \prod_{k=1}^{t/\delta t} e^{-\frac{i}{\hbar}\delta t H(k\delta t)}, \quad (4)$$

where the discretization time-step $\delta t/T_\omega \ll 1$ is chosen to ensure that $G(t)$ is independent of it. Figure 1(c) shows the maximum intensity $I_{\max}$ reached before time t at cutoff times $t = 5T_\omega$ (open red circles) and $t = 10T_\omega$ (solid blue squares), as a function of the $\mathcal{PT}$-perturbation frequency ω on the vertical axis. These results are for $\gamma/J = 0.9$, initial state localized on the first site, and a time-step $\delta t/T_\omega = 10^{-5}$. In the $\mathcal{PT}$-symmetric region, $I(t)$ undergoes bounded oscillations and therefore $I_{\max}$ is the same for the two time-cutoffs. In a sharp contrast, in the $\mathcal{PT}$-broken region, $I(t)$ increases exponentially with time and $I_{\max}$ doubles on the logarithmic scale when the cutoff is doubled. Thus, both approaches show the existence of multiple frequency windows where $\mathcal{PT}$ symmetry is broken; note that the phase-boundaries in Fig. 1(c) do not *exactly* match those in Fig. 1(b) due to the finite time-cutoff.

We remind the reader that when $\gamma/J \leq 1$, the 2×2 Hamiltonian $H(t) = i\hbar\gamma\cos(\omega t)\sigma_z - \hbar J\sigma_x$ has a purely real spectrum $\epsilon_\lambda(t) = \pm\hbar[J^2 - \gamma^2\cos^2(\omega t)]^{1/2}$ at all times, and yet, the norm of the time-evolution operator $G(t)$ is either bounded or exponential-in-time at different frequencies [27].

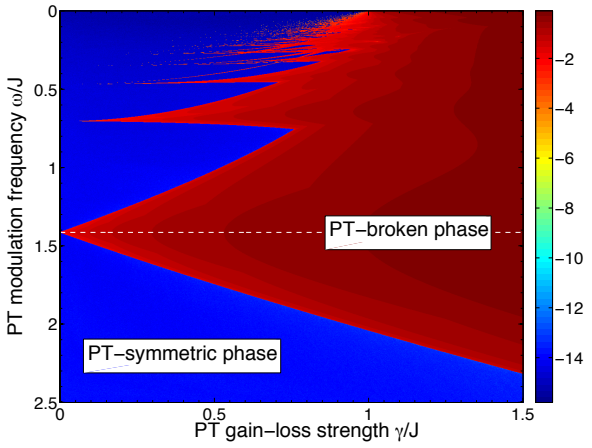

FIG. 2. (color online) $\mathcal{PT}$-symmetric phase diagram of a three-level system; shown is the base-10 log of the maximum imaginary part of the spectrum of $\mathcal{H}$. Its three features - a linearly vanishing $\mathcal{PT}$-threshold at the resonance $\omega/J = \sqrt{2} \approx 1.41$, a restored $\mathcal{PT}$-symmetric phase at high frequencies, and multiple frequency windows with $\mathcal{PT}$-symmetric and $\mathcal{PT}$-broken phases at moderate γ/J - are universal.

Figure 2 shows the $\mathcal{PT}$ phase diagram of a three-level system obtained by using 81 Floquet bands. We plot the base-10 logarithm of the largest imaginary part of eigenvalues of $\mathcal{H}$ to easily distinguish the $\mathcal{PT}$-symmetric phase (blue) and $\mathcal{PT}$-broken phase (red). For a three-level system, the unperturbed spectrum is given by $\epsilon_n = \{0, \pm\sqrt{2}J\}$, and has two resonance frequencies $\Delta_{21} = \sqrt{2}J = \Delta_{32}$ and $\Delta_{31} = 2\sqrt{2}J$. Fig. 2 shows a linearly vanishing $\gamma_{PT}(\omega)$ at the first resonance $\omega/J = \sqrt{2}$, a $\mathcal{PT}$-restored phase at high frequencies, and a number of frequency windows where $\mathcal{PT}$ symmetry is broken at moderate values of $\gamma/J \lesssim 1$. There is no $\mathcal{PT}$-broken region near the second resonance, $\omega/J = 2\sqrt{2}$ (not shown) because $V(t)$ does not connect states with same parity. Thus, the phase diagram for a three-level system shares the fundamental characteristics of that for a two-level system.

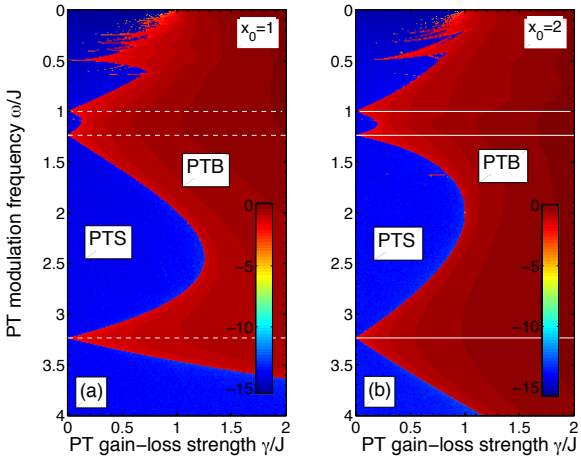

FIG. 3. (color online) Phase diagram of a 4-site lattice with gain-loss potential at the ends, $x_0 = 1$ (a), or in the center, $x_0 = 2$ (b). Both panels show a restored $\mathcal{PT}$-symmetric phase at high ω, and multiple frequency windows with PTS and PTB regions at moderate γ/J. They also show a linearly vanishing threshold $\gamma_{PT}(\omega)$ at each of the three relevant resonances, marked by dashed (a) or solid (b) white lines.

Lastly, we consider a four-level system, $N = 4$. In this case, the resonances between states with opposite parity occur at $\Delta_{21}/J = 1 = \Delta_{34}/J$, $\Delta_{23}/J = (\sqrt{5}-1) \approx 1.236$, and $\Delta_{14}/J = (\sqrt{5}+1) \approx 3.236$. There are two inequivalent locations for the gain-loss potential, $x_0 = 1$ and $x_0 = 2$, and both have the same static threshold $\gamma_{PT}/J = 1$. In the first case, only center-two of the four eigenvalues become complex at the threshold, whereas in the second case all four simultaneously become complex [33]. Figure 3 shows the $\mathcal{PT}$ phase diagram obtained with 41 Floquet bands. Both panels, (a) and (b), demonstrate the three salient features discussed earlier for both two and three-level systems.

Understanding the phase boundaries. We now derive the $\mathcal{PT}$-phase boundaries at occur at high frequencies or vanishingly small γ near a resonance. The natural time-scale for an unperturbed system is proportional to $1/J$ and its static $\mathcal{PT}$ breaking threshold is also set by J. At high frequencies $\omega/J \gg 1$, the rapidly varying potential $i\gamma\cos(\omega t)$ is replaced by its average over the characteristic time-scale, $\gamma_{\rm av} \propto (\gamma/\omega)J$. For any gain-loss strength γ, no matter how large, increasing the frequency reduces the effective strength $\gamma_{\rm av}$ and thus restores the

$\mathcal{PT}$-symmetric phase. The slope of the linear phase-boundary in the region $\omega/J \gg 1$ will depend upon the number of levels N and the location x_0 of the gain-loss potential, but the linear behavior of the phase boundary is universal.

Next we derive the cone-shaped phase boundary that occurs at small γ in the neighborhood of a resonance $\omega \sim \Delta_{nm}$. For a state $|\psi(t)\rangle = \sum_n c_n(t) \exp(-i\epsilon_n t/\hbar)|n\rangle$, the interaction-picture equation of motion for the level-occupation coefficients $c_n(t)$ is given by

$$i\partial_t c_n(t) = \sum_{m=1}^{N} V_{nm}(t) e^{+i\Delta_{nm}t} c_m(t), \quad (5)$$

$$V_{nm}(t) = i\gamma \cos(\omega t)[1-(-1)^{n+m}]\langle n|x_0\rangle\langle x_0|m\rangle. \quad (6)$$

For a two-level system, when $\omega \approx \Delta_{21} = 2J$, averaging over high-frequency terms simplifies Eq.(5) to

$$\partial_t^2 c_{1,2}(t) + \left[(\omega/2 - J)^2 - (\gamma/2)^2\right] c_{1,2}(t) = 0. \quad (7)$$

Eq.(7) implies that when $|\omega - 2J| > \gamma$, the coefficients $c_1(t)$ and $c_2(t)$ oscillate in time and remain bounded, and the system is in the $\mathcal{PT}$-symmetric phase. When $|\omega - 2J| < \gamma$, $c_{1,2}(t)$ increase with time exponentially, and the system is in the $\mathcal{PT}$-broken phase. Thus, $\mathcal{PT}$-symmetric phase boundary is given by $\gamma_{PT}(\omega) = |\omega - 2J|$, and the threshold gain-loss strength vanishes as $\omega \to \Delta_{21} = 2J$. A visual inspection of Fig. 1(a) shows that, indeed, the slope of the phase-boundary lines fanning away from $\omega = 2J$ is one. Eq.(7) also implies that along the cone-shaped phase boundary, the net intensity $I(t)$ grows quadratically with time [20, 21, 24].

When $N = 3$ a similar analysis with three equidistant levels implies that near resonance $c_2(t)$ satisfies a third-order differential equation, $\partial_t^3 c_2(t) + \left[(\omega - \sqrt{2}J)^2 - (3\gamma/4)^2\right] \partial_t c_2(t) = 0$. Therefore, the phase-boundary separating the $\mathcal{PT}$-broken region from the $\mathcal{PT}$-symmetric region is given by $\gamma_{PT}(\omega) = (4/3)|\omega - \sqrt{2}J|$. This, too, can be verified by a visual inspection of Fig. 2. Our analysis also predicts that along this phase boundary, the net intensity of an initially normalized state increases quartically with time, i.e. $I(t) \propto t^4$, because $\partial_t^3 c_2(t) = 0$. In an N-level system, our analysis is applicable to a pair of levels m, n when the $\mathcal{PT}$-perturbation frequency is close to the resonance that connects those levels, $\omega \sim \Delta_{nm}$.

Thus, *a vanishingly small $\mathcal{PT}$ perturbation induces $\mathcal{PT}$-symmetry breaking when the frequency of the perturbation is close to a resonance.* Near resonance, the spatial oscillations of a state match the gain-loss temporal oscillations; as a result, it spends most of the time on the gain-medium site, leading to an exponential growth in the net intensity.

Conclusion. In this paper, we have proposed the $\mathcal{PT}$-symmetric Rabi model. We have shown that a harmonic, gain-and-loss perturbation leads to a rich $\mathcal{PT}$ phase diagram with three salient features. Among them is the existence of multiple frequency windows in which $\mathcal{PT}$-symmetry is broken and restored. Time-dependent $\mathcal{PT}$ potentials have been extensively investigated in continuum one-dimensional optical structures [25, 26]. Our results show that such potentials are a surprising spectroscopic probe, where the phase of the system - $\mathcal{PT}$-broken or $\mathcal{PT}$-symmetric - denotes the proximity of the perturbation frequency to a resonance of the system.

Although we have focused only on few-level systems here, our results are applicable to larger lattices, particularly in the vicinity of a resonance. Deep in the $\mathcal{PT}$-broken phase, at long times, nonlinear effects also become relevant, although they do not affect our findings.

This work was supported by NSF DMR-1054020 (YJ), Department of Science and Technology, India (RM), BUCD University of Pune (PD), and University of Pune research grant BCUD/RG/9 (RP). YJ thanks the hospitality of University of Pune where this work began.

[1] J.J. Sakurai, *Modern Quantum Mechanics* (Addison Wesley, Reading, MA 1995).
[2] I.I. Rabi, Phys. Rev. **51**, 652 (1937).
[3] A.E. Siegman, *Lasers* (University Science Books, Palo Alto, CA 1986).
[4] E.T. Jaynes and F.W. Cummings, Proc. of the IEEE **51**, 89 (1963).
[5] F.W. Cummings, Phys. Rev. **140**, A 1051 (1965).
[6] P.L. Knight and P.W. Milonni, Phys. Rep. **66**, 21 (1980).
[7] B.W. Shore and P.L. Knight, J. Mod. Opt. **40**, 1195 (1993).
[8] D. Braak, Phys. Rev. Lett. **107**, 100401 (2011).
[9] M. Znojil, Phys. Rev. A **82**, 052113 (2010).
[10] M. Znojil, Phys. Lett. A **375**, 3435 (2011).
[11] O. Bendix *et al.*, Phys. Rev. Lett. **103**, 030402 (2009).
[12] L. Jin and Z. Song, Phys. Rev. A **80**, 052107 (2009).
[13] Y.N. Joglekar *et al.*, Phys. Rev. A **82**, 030103(R) (2010).
[14] Y.N. Joglekar and A. Saxena, Phys. Rev. A **83**, 050101(R) (2011).
[15] D.D. Scott and Y.N. Joglekar, Phys. Rev. A **83**, 050102(R) (2011).
[16] G. Della Valle and S. Longhi, Phys. Rev. A **87**, 022119 (2013).
[17] C.M. Bender and S. Boettcher, Phys. Rev. Lett. **80**, 5243 (1998).
[18] C.M. Bender, D.C. Brody, and H.F. Jones, Phys. Rev. Lett. **89**, 270401 (2002).
[19] C.M. Bender, Rep. Prog. Phys. **70**, 947 (2007) and references therein.
[20] Y.N. Joglekar *et al.*, Eur. Phys. J. Appl. Phys. **63**, 30001 (2013).
[21] A. Guo *et al.*, Phys. Rev. Lett. **103**, 093902 (2009).
[22] C.E. Rüter *et al.*, Nat. Phys. **6**, 192 (2010).
[23] L. Feng *et al.*, Science **333**, 729 (2011).
[24] A. Regensburger *et al.*, Nature **488**, 167 (2012).
[25] Z. Lin *et al.*, Phys. Rev. Lett. **106**, 213901 (2011).
[26] L. Feng *et al.*, Nat. Mater. **12**, 108 (2013).
[27] N. Moiseyev, Phys. Rev. A **83**, 052125 (2011).
[28] X. Luo *et al.*, Phys. Rev. Lett. **110**, 243902 (2013).

[29] G. Della Valle and S. Longhi, Phys. Rev. A **87**, 022119 (2013).
[30] G. Floquet, Ann. Sci. Ecole Norm. Sup. **12**, 47 (1883).
[31] J.H. Shirley, Phys. Rev. **138**, B979 (1965).
[32] U. Peskin and N. Moiseyev, J. Chem. Phys. **99**, 4590 (1993).
[33] Y.N. Joglekar and J.L. Barnett, Phys. Rev. A **84**, 024103 (2011).